INTERNATIONAL JOURNAL OF
NUMERICAL ANALYSIS AND MODELING
Volume 20, Number 5, Pages 647–666

doi: 10.4208/ijnam2023-1028

A NEW WEAK GALERKIN METHOD WITH WEAKLY ENFORCED DIRICHLET BOUNDARY CONDITION

DAN LI, YIQIANG LI*, AND ZHANBIN YUAN

Abstract. A new weak Galerkin method with weakly enforced Dirichlet boundary condition is proposed and analyzed for the second order elliptic problems. Two penalty terms are incorporated into the weak Galerkin method to enforce the boundary condition in the weak sense. The new numerical scheme is designed by using the locally constructed weak gradient. Optimal order error estimates are established for the numerical approximation in the energy norm and usual L^2 norm. Moreover, by using the Schur complement technique, the unknowns of the numerical scheme are only defined on the boundary of each piecewise element and an effective implementation of the reduced global system is presented. Some numerical experiments are reported to demonstrate the accuracy and efficiency of the proposed method.

Key words. weak Galerkin, finite element methods, weak gradient, second order elliptic problems, polytopal partitions.

1. Introduction

This paper is focused on the new developments of the weak Galerkin (WG) method with weakly enforced Dirichlet boundary condition. For simplicity, we consider the second order elliptic problem that finds u satisfying

$$\begin{aligned} -\nabla \cdot (a\nabla u) &= f, \quad \text{in } \Omega, \\ u &= g, \quad \text{on } \partial\Omega, \end{aligned} \tag{1}$$

where Ω is a polygonal domain in $\mathbb{R}^d (d = 2, 3)$, and the diffusion tensor $a = \{a_{ij}\}_{i,j=1}^d$ is a symmetric, uniformly positive definite matrix in $\mathbb{R}^{d\times d}$.

Various finite element methods have been proposed for the second order elliptic problems. The conforming finite element method is well known but requires the continuous piecewise polynomials on simplicial grids, which leads to the difficulty in practice. To address this difficulty, the discontinuous Galerkin methods [9], the hybrid high-order method [29], virtual element methods [1, 2] and WG methods [34, 36, 37, 47, 48] have attracted wide attention. The WG method first proposed in [34] is a natural extension of the standard finite element method through a relaxed continuity requirement for the approximating functions. Due to this weak continuity, the WG methods have some advantages such as high flexibility in both numerical approximations and mesh generations. Moreover, the WG methods are generally capable of guaranteeing the physical conservation of many problems. The WG methods have been applied to solve a wide range of PDEs including the biharmonic equation [38, 43], wave equation [15], Stokes equations [39], linear elasticity equation [20], Cahn-Hilliard equation [40], Brinkman equation [23], elliptic interface problems [24], two-phase model [13], Navier-Stokes equation [16], Maxwell's equation [25, 31]. Since then, the primal dual WG methods were proposed to simulate some challenging problems including elliptic Cauchy problem [41], second order elliptic equation in non-divergee form [11, 42], Fokker-Planck type equations [44], div-curl systems with low regularity solutions [10, 19], first order transport problems

Received by the editors on March 7, 2023 and, accepted on July 31, 2023.
2000 *Mathematics Subject Classification.* 35J50, 65N30, 65N15.

[46]. Recently, Ye and Zhang [49, 50] introduced the stabilizer free WG methods to simplify the standard WG method, which have been successfully applied to solve many partial differential equations (PDEs) including second order elliptic problems [33], Stokes equations [26], biharmonic equation [51], monotone quasilinear elliptic PDEs [52].

The enforcement of Dirichlet boundary conditions is crucial in practice. It is well known that the enforcement of the strong boundary conditions is not complicated only if the computational meshes perfectly match the solving domain of the model problems, while the implementation of all other cases is very complicated [7, 30]. For the simple variational problems, the strong enforced Dirichlet boundary conditions are easy to implement and can provide a numerical approximation with needed order of convergence so that the strong boundary conditions are usually employed in many numerical methods. However, it is difficult to obtain an accurate numerical approximation for some problems such as the interface problems [21] and Naiver-Stokes equation with low Reynolds number on coarse meshes [8]. To address these issues, the weakly enforced boundary conditions have been extensively studied. The most popular approaches include Nitsche's method [28], the penalty method [5] and Lagrange multiplier method [6].

The objective of this paper is to present the weak Galerkin method with weakly enforced Dirichlet boundary condition for the Possion equation (1). The idea is to weakly impose the boundary condition through the introduction of a Lagrange multiplier. Specifically, the WG form can be obtained by seeking $u_h \in V_h$ and $\lambda_h \in \Lambda_h$ such that

$$\begin{aligned} s(u_h, v) + (a\nabla_w u_h, \nabla_w v) - \langle \lambda_h, v\rangle_{\partial\Omega} =& (f, v), \quad \forall v \in V_h, \\ h^\alpha \langle \lambda_h, \sigma\rangle_{\partial\Omega} + \langle \sigma, u_b\rangle_{\partial\Omega} =& \langle \sigma, g\rangle_{\partial\Omega}, \ \forall \sigma \in \Lambda_h, \end{aligned} \tag{2}$$

where a Lagrangian multiplier λ_h is given by $\lambda_h = h^{-\alpha}(-u_b + Q_b g)$, and then first equation in (2) can be rewritten as

$$s(u_h, v) + (a\nabla_w u_h, \nabla_w v) + h^{-\alpha}\langle u_h, v\rangle_{\partial\Omega} = (f, v) + h^{-\alpha}\langle g, v\rangle_{\partial\Omega}, \quad \forall v \in V_h. \tag{3}$$

Different from the penalty method [5], two additional penalty terms are designed through a new Lagrangian multiplier. In addition, the generalized weak gradient is employed in the numerical algorithm. The weak enforcement of Dirichlet boundary conditions has been incorporated into various numerical methods including finite element method [17, 27], hybrid high-order method [12], virtual element method [4], extended finite element methods[45]. To the best of our knowledge, most of the existing results on the WG framework are available in the sense of strong Dirichlet boundary conditions. One such exception is the modified WG method [14] that introduced different penalty terms.

The main novelty of this paper is the following. Firstly, the new WG method with the weak enforcement of Dirichlet boundary condition is a non-trivial generalization of the classical Nitsche method. This lays the potential foundation in solving many PDEs that are difficult to enforce the Dirichlet boundary condition in the strong sense. Secondly, our numerical method allows the general polytopal partitions which makes the structure of numerical approximations and mesh generations more flexible. Moreover, the new method can provide an easy-to-implement technique for certain boundary condition. Finally, we observe from some numerical results that the maximum principle of the WG method for the model equation (1) with low regularity solutions holds true on general polytopal meshes, for which the rigorous mathematical analysis has not been developed.

This paper is organized as follows. In section 2, we simply review the definition of the weak gradient and its discrete form. Section 3 presents the WG scheme for the model equation (1) and then discusses the existence and uniqueness of the numerical approximation. Section 4 is devoted to deriving an error equation for the WG scheme. We establish some technical results in section 5. The goal of section 6 is to establish some optimal order error estimates for the numerical solution. In section 7, we present some details of the Schur complement of the WG scheme. Section 8 presents a variety of numerical experiments to confirm the developed theory. Finally, section 9 summarizes this paper and presents the future work.

2. Weak Gradient Operator

This section reviews the definitions of weak gradient and its discrete form. Let T be a polygonal region with boundary ∂T. A weak function on T refers to $v = \{v_0, v_b\}$ such that $v_0 \in L^2(T)$ and $v_b \in L^2(\partial T)$. The v_0 and v_b are intended for the values of v in the interior of T and on the boundary of T, respectively. It should be pointed out that v_b and v_0 are completely independent although $v_b = v_0|_{\partial T}$ is a feasible choice.

Denote by $\mathcal{W}(T)$ the weak function space on T given by

$$\mathcal{W}(T) = \{v = \{v_0, v_b\} : v_0 \in L^2(T), v_b \in L^2(\partial T)\}.$$

Definition 2.1. [34] *(Weak gradient) For any weak function $v \in \mathcal{W}(T)$, the weak gradient, denoted by $\nabla_{w,T} v$ for v, is defined as a linear function in the dual space of $[H^1(T)]^d$ satisfying*

$$(\nabla_{w,T} v, \boldsymbol{\psi})_T = -(v_0, \nabla \cdot \boldsymbol{\psi})_T + \langle v_b, \boldsymbol{\psi} \cdot \boldsymbol{n} \rangle_{\partial T}, \quad \forall \boldsymbol{\psi} \in [H^1(T)]^d,$$

where $\boldsymbol{n}$ is the unit outward normal vector to ∂T.

For any given integer $r \geq 0$, $P_r(T)$ is the set of polynomial spaces on T with total degrees no more than r.

Definition 2.2. [34] *(Discrete weak gradient) The discrete weak gradient for any weak function $v \in \mathcal{W}(T)$, denoted by $\nabla_{w,r,T} v$, is defined as a unique vector-valued polynomial in $[P_r(T)]^d$ such that*

$$(\nabla_{w,r,T} v, \boldsymbol{\psi})_T = -(v_0, \nabla \cdot \boldsymbol{\psi})_T + \langle v_b, \boldsymbol{\psi} \cdot \boldsymbol{n} \rangle_{\partial T}, \quad \forall \boldsymbol{\psi} \in [P_r(T)]^d. \tag{4}$$

3. Weak Galerkin Scheme

This section presents the WG method for the equation (1) and then discusses the existence and uniqueness of the numerical approximation. Let $\mathcal{T}_h$ be a general polygonal or polyhedral partition of Ω that satisfies the regular assumptions described as in [37]. Denote by $\mathcal{E}_h$ the set of all edges or flat faces in $\mathcal{T}_h$. Denote by $\mathcal{E}_h^0 = \mathcal{E}_h \setminus \partial\Omega$ the set of all interior edges or faces and $\mathcal{E}_{\partial\Omega} = \mathcal{E}_h \cap \partial\Omega$ the set of all boundary edges or faces, respectively. For each element $T \in \mathcal{T}_h$, let h_T be the mesh size of T and $h = \max_{T \in \mathcal{T}_h} h_T$ be the mesh size of $\mathcal{T}_h$. Similarly, on each edge or face $e \in \mathcal{E}_{\partial\Omega}$, h_e means the mesh size of e.

For integer $k \geq 1$, denote by $V_k(T)$ the piecewise weak function space on T given by

$$V_k(T) = \{v = \{v_0, v_b\} : v_0 \in P_k(T), v_b \in P_{k-1}(e),\ T \in \mathcal{T}_h,\ e \subset \partial T\}.$$

By patching the local finite element $V_k(T)$ over all the elements $T \in \mathcal{T}_h$ through a unique value v_b on $\mathcal{E}_h^0$, we build a global finite element space V_h; i.e.,

$$V_h = \{v = \{v_0, v_b\} : v|_T \in V_k(T), \quad T \in \mathcal{T}_h\}.$$

For simplicity, ∇_w is the discrete weak gradient operator $\nabla_{w,k-1,T}$ defined by (4) with $r = k-1$; i.e.,

$$(\nabla_w v)|_T = \nabla_{w,k-1,T}(v|_T),\ v \in V_h.$$

For any $w, v \in V_h$, two bilinear forms are given as follows

$$\begin{aligned}(a\nabla_w w, \nabla_w v)_{\mathcal{T}_h} &= \sum_{T\in\mathcal{T}_h} (a\nabla_w w, \nabla_w v)_T,\\ s(w,v) &= \sum_{T\in\mathcal{T}_h} h_T^{-1}\langle Q_b w_0 - w_b, Q_b v_0 - v_b\rangle_{\partial T},\end{aligned} \tag{5}$$

where Q_b is the usual L^2 projection operator from $L^2(e)$ to $P_{k-1}(e)$.

To weakly enforce the Dirichlet boundary condition, we introduce the following bilinear form:

$$b(w_b, v_b) = \sum_{e\in\mathcal{E}_{\partial\Omega}} h_e^{-\alpha}\langle w_b, v_b\rangle_e,\ w_b, v_b \in V_h, \tag{6}$$

where $\alpha \in \mathbb{R}$.

Weak Galerkin scheme 1. *A numerical approximation for equation* (1) *can be obtained by seeking* $u_h = \{u_0, u_b\} \in V_h$ *such that*

$$(a\nabla_w u_h, \nabla_w v)_{\mathcal{T}_h} + s(u_h, v) + b(u_b, v_b) = (f, v_0) + b(Q_b g, v_b),\ \forall v \in V_h, \tag{7}$$

where $b(u_b, v_b)$ *and* $b(Q_b g, v_b)$ *are defined by* (6) *or its equivalent form.*

Remark 3.1. *Compared* (7) *with the WG scheme in* [22]*, a weakly enforced Dirichlet boundary condition is employed. It should be pointed out that the numerical approximation* u_b *arising from* (7) *is given by* $u_b = Q_b g + \varepsilon_b$ *with unknown perturbation* ε_b *. To this end, multiplying the linear system* (7) *by* h_e^α *gives rise to the approximation* u_b *when the mesh size* h_e *is small enough .*

To reduce the computational complexity of (7), we review the following equivalence result.

Lemma 3.1. *For any* $v_b \in V_h$*, the bilinear form* $\langle v_b, v_b\rangle_{\partial\Omega}$ *is spectrally equivalent to the corresponding discrete form* $\sum_{e\in\mathcal{E}_{\partial\Omega}}\sum_{i=1}^m h_e^{d-1}|v_b(A_i)|^2$ *in the sense that there exist two constants* C_1 *and* C_2 *such that*

$$C_1 \sum_{e\in\mathcal{E}_{\partial\Omega}}\sum_{i=1}^m h_e^{d-1}|v_b(A_i)|^2 \le \langle v_b, v_b\rangle_{\partial\Omega} \le C_2 \sum_{e\in\mathcal{E}_{\partial\Omega}}\sum_{i=1}^m h_e^{d-1}|v_b(A_i)|^2, \tag{8}$$

where $v_b(A_i)$ *represents the value of* v_b *at the vertice* $A_i = (x_i, y_i)$ *or* $A_i = (x_i, y_i, z_i)$ *on* $e \in \mathcal{E}_{\partial\Omega} \cap \partial T$*, and the integer* m *is* $m = k$ *in two dimension and* $m = k(k+1)/2$ *in three dimension, respectively.*

Proof. Similar proof can be found in [35] in details. □

For any $w_b, v_b \in V_h$, from (8), the bilinear form $b(w_b, v_b)$ given by (6) can be reformulated as follows

$$b(w_b, v_b) = \sum_{e\in\mathcal{E}_{\partial\Omega}}\sum_{i=1}^m h_e^{d-1-\alpha} w_b v_b(A_i).$$

For any $v \in V_h$, we introduce

$$|\!|\!| v |\!|\!|^2 = (a\nabla_w v, \nabla_w v)_{\mathcal{T}_h} + s(v, v) + b(v_b, v_b). \tag{9}$$

Lemma 3.2. *For any* $v \in V_h$*,* $|\!|\!| v |\!|\!|$ *defined by* (9) *is a norm.*

Proof. It suffices to prove that the positivity property for $|||v|||$ holds true. To this end, assume that $|||v||| = 0$. By using (9) and the properties of diffusive tensor a gives $\nabla_w v = 0$ on each T, $Q_b v_0 = v_b$ on each ∂T and $v_b = 0$ on each $\partial\Omega$. It follows from (4) and integration by parts that for any $\boldsymbol{q} \in [P_{k-1}(T)]^d$

$$\begin{aligned} 0 &= (\nabla_w v, \boldsymbol{q})_T \\ &= (\nabla v_0, \boldsymbol{q})_T - \langle v_0 - v_b, \boldsymbol{q}\cdot\mathbf{n}\rangle_{\partial T} \\ &= (\nabla v_0, \boldsymbol{q})_T - \langle Q_b v_0 - v_b, \boldsymbol{q}\cdot\mathbf{n}\rangle_{\partial T} \\ &= (\nabla v_0, \boldsymbol{q})_T, \end{aligned}$$

which implies $\nabla v_0 = 0$ on each T. Thus, $v_0 = const$ on each T. This, together with $Q_b v_0 = v_0$ and $Q_b v_0 = v_b$ on each ∂T, leads to $v_0 \in C^0(\Omega)$. From $v_b = 0$ on $e \subset \partial\Omega$, we have $v_0 = 0$ in Ω and further $v_b = 0$ on each ∂T. This completes the proof. □

Lemma 3.3. *The weak Galerkin scheme* (7) *has one and only one numerical solution.*

Proof. It follows from (7) that the coefficient matrix (7) is symmetric and positive definite, which verifies the existence of the numerical solution. Next, it suffices to prove the uniqueness of the numerical approximation. To this end, assume that $u_h^{(1)}$ and $u_h^{(2)}$ are two different solutions of the WG scheme (7), there holds

$$(a\nabla_w(u_h^{(1)} - u_h^{(2)}), \nabla_w v)_{\mathcal{T}_h} + s(u_h^{(1)} - u_h^{(2)}, v) + b(u_h^{(1)} - u_h^{(2)}, v_b) = 0$$

for any $v \in V_h$. By letting $v = u_h^{(1)} - u_h^{(2)}$ in the above equation and using Lemma 3.2 leads to $u_h^{(1)} = u_h^{(2)}$. This completes the proof. □

4. Error Equation

The goal of this section is to derive an error equation for the WG scheme (7). To this end, we introduce some projection operators. On each element $T \in \mathcal{T}_h$, denote by Q_0 the usual L^2 projection operator onto $P_k(T)$. For any $\phi \in H^1(\Omega)$, by combining Q_0 with Q_b gives rise to a projection $Q_h\phi = \{Q_0\phi, Q_b\phi\}$. Similarly, denote by $\mathbb{Q}_h$ the usual L^2 projection operator mapping from $[L^2(T)]^d$ to $[P_{k-1}(T)]^d$.

Lemma 4.1. [22] *For any $\phi \in H^1(T)$, we have the following commutative property*

$$\nabla_w(Q_h\phi) = \mathbb{Q}_h\nabla\phi.$$

Let u be the exact solution of equation (1) and u_h be the numerical approximation of the WG scheme (7). e_h is denoted as the difference between the L^2 projection of the exact solution and the numerical approximation given by

$$e_h = \{e_0, e_b\} = \{Q_0 u - u_0, Q_b u - u_b\}.$$

For simplicity of analysis, assume that the diffusion tensor a in (1) is a piecewise constant matrix. The following results can be easily extended to the WG scheme (7) with the variable diffusion tensor if the matrix a is enough smooth.

Lemma 4.2. *For any $v \in V_h$, the error function e_h satisfies the following equation*

$$(a\nabla_w e_h, \nabla_w v)_{\mathcal{T}_h} + s(e_h, v) + b(e_b, v_b) = s(Q_h u, v) + \ell_u(v) + \langle a\nabla u\cdot\boldsymbol{n}, v_b\rangle_{\partial\Omega}, \tag{10}$$

where the linear function $\ell_u(v)$ is given by

$$\ell_u(v) = \sum_{T\in\mathcal{T}_h} \langle v_0 - v_b, a(I - \mathbb{Q}_h)\nabla u\cdot\boldsymbol{n}\rangle_{\partial T}. \tag{11}$$

Proof. It follows from Lemma 4.1, (4) with $\boldsymbol{q} = a\mathbb{Q}_h\nabla u$ and integration by parts that

$$\begin{aligned}(a\nabla_w Q_h u, \nabla_w v)_{\mathcal{T}_h} =& (a\mathbb{Q}_h\nabla u, \nabla_w v)_{\mathcal{T}_h}\\ =& -\sum_{T\in\mathcal{T}_h}(v_0, \nabla\cdot(a\mathbb{Q}_h\nabla u))_T + \sum_{T\in\mathcal{T}_h}\langle v_b, a\mathbb{Q}_h\nabla u\cdot\mathbf{n}\rangle_{\partial T}\\ =& \sum_{T\in\mathcal{T}_h}(\nabla v_0, a\mathbb{Q}_h\nabla u)_T + \sum_{T\in\mathcal{T}_h}\langle v_b - v_0, a\mathbb{Q}_h\nabla u\cdot\mathbf{n}\rangle_{\partial T}\\ =& (\nabla v_0, a\nabla u) + \sum_{T\in\mathcal{T}_h}\langle v_b - v_0, a\mathbb{Q}_h\nabla u\cdot\mathbf{n}\rangle_{\partial T},\end{aligned} \tag{12}$$

where the property of $\mathbb{Q}_h$ is used in the last step.

To deal with the first term on the right hand of (12), we test the model equation (1) against v_0 and then use integration by parts to obtain

$$\begin{aligned}(f, v_0) =& -(\nabla\cdot(a\nabla u), v_0)\\ =& (a\nabla u, \nabla v_0) - \sum_{T\in\mathcal{T}_h}\langle a\nabla u\cdot\mathbf{n}, v_0\rangle_{\partial T}\\ =& (a\nabla u, \nabla v_0) - \sum_{T\in\mathcal{T}_h}\langle a\nabla u\cdot\mathbf{n}, v_0 - v_b\rangle_{\partial T} - \langle a\nabla u\cdot\mathbf{n}, v_b\rangle_{\partial\Omega},\end{aligned} \tag{13}$$

where $\sum_{e\in\mathcal{E}_h^0}\langle a\nabla u\cdot\mathbf{n}, v_b\rangle_e = 0$ is used since v_b is single valued on each $e\in\mathcal{E}_h$.

Substituting (13) into (12) and then using the WG scheme (7) give

$$\begin{aligned}&(a\nabla_w Q_h u, \nabla_w v)_{\mathcal{T}_h}\\ =& (f, v_0) + \sum_{T\in\mathcal{T}_h}\langle v_0 - v_b, a(I - \mathbb{Q}_h)\nabla u\cdot\mathbf{n}\rangle_{\partial T} + \langle a\nabla u\cdot\mathbf{n}, v_b\rangle_{\partial\Omega}\\ =& (a\nabla_w u_h, \nabla_w v)_{\mathcal{T}_h} + s(u_h, v) + b(u_b, v_b) - b(Q_b g, v_b) + \ell_u(v) + \langle a\nabla u\cdot\mathbf{n}, v_b\rangle_{\partial\Omega}\\ =& (a\nabla_w u_h, \nabla_w v)_{\mathcal{T}_h} + s(Q_h u - e_h, v) - b(e_b, v_b) + b(Q_b u - Q_b g, v_b) + \ell_u(v)\\ &+ \langle a\nabla u\cdot\mathbf{n}, v_b\rangle_{\partial\Omega}\\ =& (a\nabla_w u_h, \nabla_w v)_{\mathcal{T}_h} - s(e_h, v) - b(e_b, v_b) + s(Q_h u, v) + \ell_u(v) + \langle a\nabla u\cdot\mathbf{n}, v_b\rangle_{\partial\Omega},\end{aligned}$$

which, together with $u = g$ on $\partial\Omega$, leads to Lemma 4.2. This completes the proof. □

5. Technical Results

This section is to derive some technical results to be used in the following convergence analysis.

Assume $\mathcal{T}_h$ is a regular partition presented in [37]. Then, for any $T\in\mathcal{T}_h$ and $\phi\in H^1(T)$, the following trace inequality holds true

$$\|\phi\|_{\partial T}^2 \le C(h_T^{-1}\|\phi\|_T^2 + h_T\|\nabla\phi\|_T^2). \tag{14}$$

Moreover, if ϕ is a polynomial on $T\in\mathcal{T}_h$, we have

$$\|\phi\|_{\partial T}^2 \le Ch_T^{-1}\|\phi\|_T^2. \tag{15}$$

Lemma 5.1. [37] *Let $\mathcal{T}_h$ be a regular partition of Ω that satisfies the assumptions described as in* [37]*. Then, for any $\phi\in H^{k+1}(\Omega)$, there holds*

$$\sum_{T\in\mathcal{T}_h}(\|\phi - Q_0\phi\|_T^2 + h_T^2\|\nabla(\phi - Q_0\phi)\|_T^2) \le Ch^{2(k+1)}\|\phi\|_{k+1}^2,$$

$$\sum_{T\in\mathcal{T}_h}(\|\phi - \mathbb{Q}_h\phi\|_T^2 + h_T^2\|\nabla(\phi - \mathbb{Q}_h\phi)\|_T^2) \le Ch^{2k}\|\phi\|_{k+1}^2.$$

Lemma 5.2. [22] *For any $v \in V_h$, we have the following estimate*

$$\|\nabla v_0\| \leq C|\!|\!|v|\!|\!|.$$

Lemma 5.3. *For any $u \in H^{k+1}(\Omega)$ and $v \in V_h$, there exists a constant C such that*

$$|s(Q_h u, v)| \leq Ch^k \|u\|_{k+1} |\!|\!|v|\!|\!|, \tag{16}$$

$$|\ell_u(v)| \leq Ch^k \|u\|_{k+1} |\!|\!|v|\!|\!|, \tag{17}$$

$$|\langle a\nabla u \cdot \boldsymbol{n}, v_b\rangle_{\partial\Omega}| \leq Ch^{\frac{\alpha}{2}} \|a\nabla u \cdot \boldsymbol{n}\|_{\partial\Omega} |\!|\!|v|\!|\!|. \tag{18}$$

Proof. To derive (16), by using the Cauchy-Schwarz inequality, (14) and Lemma 5.1, we have

$$\begin{aligned}
&|s(Q_h u, v)| \\
=&|\sum_{T\in\mathcal{T}_h} h_T^{-1}\langle Q_b(Q_0 u) - Q_b u, Q_b v_0 - v_b\rangle_{\partial T}| \\
\leq& C\Big(\sum_{T\in\mathcal{T}_h} h_T^{-1}\|Q_0 u - u\|_{\partial T}^2\Big)^{\frac{1}{2}}\Big(\sum_{T\in\mathcal{T}_h} h_T^{-1}\|Q_b v_0 - v_b\|_{\partial T}^2\Big)^{\frac{1}{2}} \\
\leq& Ch^k\|u\|_{k+1}|\!|\!|v|\!|\!|,
\end{aligned}$$

which leads to the desired error estimate.

From the Cauchy-Schwarz inequality, (14), Lemmas 5.1 and 5.2, $\ell_u(v)$ given by (17) we obtain

$$\begin{aligned}
|\ell_u(v)| =& |\sum_{T\in\mathcal{T}_h} \langle v_0 - v_b, a(I - \mathbb{Q}_h)\nabla u \cdot \mathbf{n}\rangle_{\partial T}| \\
\leq& C\Big(\sum_{T\in\mathcal{T}_h} \|v_0 - v_b\|_{\partial T}^2\Big)^{\frac{1}{2}}\Big(\sum_{T\in\mathcal{T}_h} \|a(I - \mathbb{Q}_h)\nabla u \cdot \mathbf{n}\|_{\partial T}^2\Big)^{\frac{1}{2}} \\
\leq& C\Big(\sum_{T\in\mathcal{T}_h} \|Q_b v_0 - v_b\|_{\partial T}^2 + \sum_{T\in\mathcal{T}_h} \|v_0 - Q_b v_0\|_{\partial T}^2\Big)^{\frac{1}{2}} h^{\frac{2k-1}{2}}\|u\|_{k+1} \\
\leq& Ch^{\frac{2k-1}{2}}\|u\|_{k+1}\Big(h|\!|\!|v|\!|\!|^2 + h\|\nabla v_0\|^2\Big)^{\frac{1}{2}} \\
\leq& Ch^k\|u\|_{k+1}|\!|\!|v|\!|\!|,
\end{aligned}$$

which implies the desired estimate.

For (18), using (6) and (9) yields

$$\begin{aligned}
|\langle a\nabla u \cdot \mathbf{n}, v_b\rangle_{\partial\Omega}| \leq& Ch^{\frac{\alpha}{2}}\|a\nabla u \cdot \mathbf{n}\|_{\partial\Omega} h^{\frac{-\alpha}{2}}\|v_b\|_{\partial\Omega} \\
\leq& Ch^{\frac{\alpha}{2}}\|a\nabla u \cdot \mathbf{n}\|_{\partial\Omega}|\!|\!|v|\!|\!|.
\end{aligned}$$

This completes the proof of the lemma. □

6. Error Estimates

This section is devoted to establishing some error estimates for the numerical approximation in the energy norm and L^2 norm.

Theorem 6.1. *Assume that $u \in H^{k+1}(\Omega)$ is the exact solution of the equation* (1). *Let $u_h \in V_h$ be the numerical approximation of the WG scheme* (7). *Then, we have*

$$|\!|\!|e_h|\!|\!| \leq C(h^k\|u\|_{k+1} + h^{\frac{\alpha}{2}}\|a\nabla u \cdot \boldsymbol{n}\|_{\partial\Omega}),$$

which implies that $\alpha = 2k$ is the optimal exponent.

Proof. Let $v = e_h$ in (10), we get

$$(a\nabla_w e_h, \nabla_w e_h)_{\mathcal{T}_h} + s(e_h, e_h) + b(e_b, e_b) = s(Q_h u, e_h) + \ell_u(e_h) + \langle a\nabla u \cdot \mathbf{n}, e_b\rangle_{\partial\Omega}.$$

From (9) and Lemma 5.3 with $v = e_h$, there yields

$$|||e_h|||^2 \leq C(h^k \|u\|_{k+1} + h^{\frac{\alpha}{2}} \|a\nabla u \cdot \mathbf{n}\|_{\partial\Omega})|||e_h|||,$$

This completes the proof of the theorem. □

In order to establish an optimal order error estimate e_0 in the L^2 norm, the following dual problem is introduced as:

$$\begin{aligned} -\nabla \cdot (a\nabla\Phi) &= e_0, \text{ in } \Omega, \\ \Phi &= 0, \quad \text{on } \partial\Omega. \end{aligned} \tag{19}$$

If problem (19) satisfies the H^2-regularity property, then there exists a general constant C such that

$$\|\Phi\|_2 \leq C\|e_0\|. \tag{20}$$

Theorem 6.2. *Let $u \in H^{k+1}(\Omega)$ be the exact solution of equation* (1) *and $u_h \in V_h$ be the numerical approximation of the WG scheme* (7)*, respectively. If the dual problem* (19) *has the H^2-regularity property* (20)*. Then, we have the following error estimate*

$$\|e_0\| \leq C(h^{k+1}\|u\|_{k+1} + (h + h^{\frac{\alpha}{2}})|||e_h|||),$$

which implies the optimal exponent $\alpha = 2k$.

Proof. By testing the dual problem (19) against e_0 and integrating by parts, we obtain

$$\begin{aligned} \|e_0\|^2 =& (-\nabla \cdot (a\nabla\Phi), e_0) \\ =& \sum_{T\in\mathcal{T}_h} (a\nabla\Phi, \nabla e_0)_T - \sum_{T\in\mathcal{T}_h} \langle a\nabla\Phi \cdot \mathbf{n}, e_0\rangle_{\partial T} \\ =& \sum_{T\in\mathcal{T}_h} (a\nabla\Phi, \nabla e_0)_T - \sum_{T\in\mathcal{T}_h} \langle a\nabla\Phi \cdot \mathbf{n}, e_0 - e_b\rangle_{\partial T} - \langle a\nabla\Phi \cdot \mathbf{n}, e_b\rangle_{\partial\Omega}. \end{aligned} \tag{21}$$

To analyze the first right term on the right hand side of (21), by choosing $u = \Phi$ and $v = e_h$ in (12), we obtain

$$(a\nabla\Phi, \nabla e_0) = (a\nabla_w Q_h\Phi, \nabla_w e_h)_{\mathcal{T}_h} - \sum_{T\in\mathcal{T}_h} \langle e_b - e_0, a\mathbb{Q}_h\nabla\Phi \cdot \mathbf{n}\rangle_{\partial T}. \tag{22}$$

Substituting (22) into (21) and using (10) with $v = Q_h\Phi$, we have

$$\begin{aligned} \|e_0\|^2 =& (a\nabla_w Q_h\Phi, \nabla_w e_h)_{\mathcal{T}_h} - \sum_{T\in\mathcal{T}_h} \langle e_b - e_0, a(\mathbb{Q}_h - I)\nabla\Phi \cdot \mathbf{n}\rangle_{\partial T} \\ & - \langle a\nabla\Phi \cdot \mathbf{n}, e_b\rangle_{\partial\Omega} \\ =& s(Q_h u, Q_h\Phi) + \ell_u(Q_h\Phi) - s(e_h, Q_h\Phi) - b(e_b, Q_b\Phi) \\ & + \langle a\nabla u \cdot \mathbf{n}, Q_b\Phi\rangle_{\partial\Omega} - \ell_\Phi(e_h) - \langle a\nabla\Phi \cdot \mathbf{n}, e_b\rangle_{\partial\Omega} \\ =& s(Q_h u, Q_h\Phi) + \ell_u(Q_h\Phi) - s(e_h, Q_h\Phi) - \ell_\Phi(e_h) - \langle a\nabla\Phi \cdot \mathbf{n}, e_b\rangle_{\partial\Omega}, \end{aligned} \tag{23}$$

where $\Phi = 0$ on $\partial\Omega$ is also used.

Next, it remains to deal with the five terms on the right hand side of (23) one by one. To derive the first term, it follows from the Cauchy-Schwarz inequality, (14)

and Lemma 5.1 that

$$
\begin{aligned}
|s(Q_h u, Q_h\Phi)| =& |\sum_{T\in\mathcal{T}_h} h_T^{-1}\langle Q_b(Q_0 u) - Q_b u, Q_b(Q_0\Phi) - Q_b\Phi\rangle_{\partial T}| \\
\le& C\Big(\sum_{T\in\mathcal{T}_h} h_T^{-1}\|Q_0 u - u\|_{\partial T}^2\Big)^{\frac{1}{2}}\Big(\sum_{T\in\mathcal{T}_h} h_T^{-1}\|Q_0\Phi - \Phi\|_{\partial T}^2\Big)^{\frac{1}{2}} \\
\le& Ch^{k+1}\|u\|_{k+1}\|\Phi\|_2 \\
\le& Ch^{k+1}\|u\|_{k+1}\|e_0\|,
\end{aligned} \tag{24}
$$

where the regularity property (20) is also used in the last step.

For the second term, the Cauchy-Schwarz inequality, (14), Lemma 5.1 and the regularity property (20) are used to obtain

$$
\begin{aligned}
|\ell_u(Q_h\Phi)| =& |\sum_{T\in\mathcal{T}_h} \langle Q_0\Phi - Q_b\Phi, a(I-\mathbb{Q}_h)\nabla u\cdot\mathbf{n}\rangle_{\partial T}| \\
\le& C\Big(\sum_{T\in\mathcal{T}_h} \|Q_0\Phi - \Phi\|_{\partial T}^2\Big)^{\frac{1}{2}}\Big(\sum_{T\in\mathcal{T}_h} \|a(I-\mathbb{Q}_h)\nabla u\cdot\mathbf{n}\|_{\partial T}^2\Big)^{\frac{1}{2}} \\
\le& Ch^{k+1}\|u\|_{k+1}\|\Phi\|_2 \\
\le& Ch^{k+1}\|u\|_{k+1}\|e_0\|.
\end{aligned} \tag{25}
$$

To derive the last three terms, using the similar arguments as in Lemma 5.3 and (20) gives

$$
\begin{aligned}
|s(Q_h\Phi, e_h)| \le& Ch\|e_0\|\|\!|e_h|\!\|, \\
|\ell_\Phi(e_h)| \le& Ch\|e_0\|\|\!|e_h|\!\|, \\
|\langle a\nabla\Phi\cdot\mathbf{n}, e_b\rangle_{\partial\Omega}| \le& Ch^{\frac{\alpha}{2}}\|a\nabla\Phi\cdot\mathbf{n}\|_{\partial\Omega}\|\!|e_h|\!\| \\
\le& Ch^{\frac{\alpha}{2}}\|\Phi\|_2\|\!|e_h|\!\| \\
\le& Ch^{\frac{\alpha}{2}}\|e_0\|\|\!|e_h|\!\|,
\end{aligned}
$$

where we also used (9) and the trace theorem for Sobolev space [3].

Finally, substituting (24)-(25) and the above three estimates into (23) yields

$$
\|e_0\|^2 \le C(h^{k+1}\|u\|_{k+1} + (h + h^{\frac{\alpha}{2}})\|\!|e_h|\!\|)\|e_0\|.
$$

This completes the proof. □

Let us introduce the following norm defined on the all edges or faces:

$$
\|e_b\|_{\mathcal{E}_h} = \Big(\sum_{T\in\mathcal{T}_h} h_T\|e_b\|_{\partial T}^2\Big)^{\frac{1}{2}}.
$$

Theorem 6.3. *Under the assumptions of Theorem 6.2, there holds*

$$
\|e_b\|_{\mathcal{E}_h} \le C(h^{k+1}\|u\|_{k+1} + (h + h^{\frac{\alpha}{2}})\|\!|e_h|\!\|).
$$

Proof. By the triangle inequality and (15), we can obtain

$$
\begin{aligned}
\|e_b\|_{\mathcal{E}_h} =& \Big(\sum_{T\in\mathcal{T}_h} h_T\|e_b\|_{\partial T}^2\Big)^{\frac{1}{2}} \\
\le& C\Big(\sum_{T\in\mathcal{T}_h} h_T\|e_b - Q_b e_0\|_{\partial T}^2 + \sum_{T\in\mathcal{T}_h} h_T\|Q_b e_0\|_{\partial T}^2\Big)^{\frac{1}{2}} \\
\le& C\Big(h^2\|\!|e_h|\!\|^2 + \|e_0\|\Big)^{\frac{1}{2}},
\end{aligned}
$$

which, together with Theorems 6.1 and 6.2, leads to the desired result. This completes the proof. □

7. Schur Complement of Weak Galerkin Method

To present an effective implementation of the Schur complement of the WG scheme (7), we recall that the WG solution u_h satisfies

$$(a\nabla_w u_h, \nabla_w v)_{\mathcal{T}_h} + s(u_h, v) + b(u_b, v_b) = (f, v_0) + b(Q_b g, v_b),\ \forall v \in V_h. \tag{26}$$

Setting $v = \{v_0, 0\}$ in (26) yields

$$(a\nabla_w u_h, \nabla_w v)_{\mathcal{T}_h} + s(u_h, v) = (f, v_0). \tag{27}$$

Taking $v = \{0, v_b\}$ in (26) gives

$$(a\nabla_w u_h, \nabla_w v)_{\mathcal{T}_h} + s(u_h, v) + b(u_b, v_b) = b(Q_b g, v_b). \tag{28}$$

It follows from (27) that for a given numerical approximation u_b on each ∂T, the unknown variable u_0 can be written as

$$u_0 = u_0(u_b, f). \tag{29}$$

From the principle of superposition, the WG solution $u_h = \{u_0, u_b\}$ can be reformulated as follows

$$\{u_0, u_b\} = \{u_0(u_b, f), u_b\} = \{u_0(0, f), 0\} + \{u_0(u_b, 0), u_b\}.$$

Next, substituting the above formulation into (28), we arrive at

$$\begin{aligned} &(a\nabla_w\{u_0(u_b,0),u_b\}, \nabla_w v)_{\mathcal{T}_h} + s(\nabla_w\{u_0(u_b,0),u_b\}, v) + b(u_b, v_b) \\ =&b(Q_b g, v_b) - (a\nabla_w\{u_0(0,f),0\}, \nabla_w v)_{\mathcal{T}_h} - s(\nabla_w\{u_0(0,f),0\}, v) \end{aligned} \tag{30}$$

for any $v = \{0, v_b\} \in V_h$. From which the unknown variable u_b can be obtained. Then u_0 can be solved by (29).

For simplicity, the implementation of the Schur complement of WG scheme (27)-(28) is summarized as follows:

Step 1 Solve the equation (27) to get $u_0 = u_0(u_b, f)$.
Step 2 Substitute $u_0 = u_0(u_b, f)$ into (30) to obtain u_b.
Step 3 Recover u_0 by $u_0 = u_0(u_b, f)$ with u_b.

Remark 7.1. *Note that the solution of the Schur complement of the WG scheme* (27)-(28) *is the numerical approximation of the WG scheme* (7)*, since the uniqueness of numerical solution of* (7) *implies the fact. Moreover, the Schur component of the WG methods can significantly reduce the degrees of freedom, especially for the model problems with high order derivatives in high dimensions. Furthermore, the global system can be obtained by calculating the local system on each finite element in a completely independent manner and then integrated them over all the elements* $T \in \mathcal{T}_h$.

The matrix form of (27)-(28) shall be presented to show further implement the Schur complement of the WG methods. We only demonstrate the details on a typical element $T \in \mathcal{T}_h$ because of the similarity for others.

For each $T \in \mathcal{T}_h$, we introduce the following matrices

$$\begin{aligned} &A_{0,0} = [(a\nabla_w\{\phi_{0j}, 0\}, \nabla_w\{\phi_{0i}, 0\})]_{i,j,T},\ A_{0,b} = [(a\nabla_w\{0, \phi_{bj}\}, \nabla_w\{\phi_{0i}, 0\})]_{i,j,T}, \\ &A_{b,0} = [(a\nabla_w\{\phi_{0j}, 0\}, \nabla_w\{0, \phi_{bi}\})]_{i,j,T},\ A_{b,b} = [(a\nabla_w\{0, \phi_{bj}\}, \nabla_w\{0, \phi_{bi}\})]_{i,j,T}, \\ &S_{0,0} = [s(\{\phi_{0j}, 0\}, \{\phi_{0i}, 0\})]_{i,j,T},\ S_{0,b} = [s(\{0, \phi_{bj}\}, \{\phi_{0i}, 0\})]_{i,j,T}, \\ &S_{b,0} = [s(\{\phi_{0j}, 0\}, \{0, \phi_{bi}\})]_{i,j,T},\ S_{b,b} = [s(\{0, \phi_{bj}\}, \{0, \phi_{bi}\})]_{i,j,T}, \\ &B_{\partial\Omega} = [b(\phi_{bj}, \phi_{bi})]_{i,j,T},\ F_0 = [(f, \phi_{0i})]_{i,T},\ F_{\partial\Omega} = [b(Q_b g, \phi_{b,j})]_{i,T}, \end{aligned}$$

in which $\{\phi_{0i}\}$ and $\{\phi_{bj}\}$ are the sets of basis functions for the first and second components of weak function in the finite element space $V_k(T)$, respectively.

By substituting the above matrices into the WG scheme (26), we have

$$\begin{pmatrix} A_{0,0}+S_{0,0} & A_{0,b}+S_{0,b} \\ A_{b,0}+S_{b,0} & A_{b,b}+S_{b,b}+B_{\partial\Omega} \end{pmatrix} \begin{pmatrix} u_0 \\ u_b \end{pmatrix} = \begin{pmatrix} F_0 \\ F_{\partial\Omega} \end{pmatrix},$$

from which, we get

$$u_0 = (A_{0,0}+S_{0,0})^{-1}(F_0 - (A_{0,b}+S_{0,b})u_b). \tag{31}$$

Substituting (31) into the second equation in the matrix form of the WG scheme gives

$$\begin{aligned} &\Big((A_{b,b}+S_{b,b}+B_{\partial\Omega}) - (A_{b,0}+S_{b,0})(A_{0,0}+S_{0,0})^{-1}(A_{0,b}+S_{0,b})\Big)u_b \\ =&F_{\partial\Omega} - (A_{b,0}+S_{b,0})(A_{0,0}+S_{0,0})^{-1}F_0, \end{aligned}$$

which leads to u_b, and u_0 can be solved by equation (31) additionally.

8. Numerical Experiments

In this section, some numerical experiments are reported to confirm the convergence theory established in previous sections.

For simplicity, the piecewise linear finite element V_h with $k = 1$ and quadratic element V_h with $k = 2$ are employed. To demonstrate the efficiency and flexibility of the WG methods, various numerical experiments with smooth and low regularity solutions are conducted on both the convex domain $\Omega_1 = (0,1)^2$ and the non-convex domain Ω_2 with vertices $B_1 = (-1,-1)$, $B_2 = (0,-1)$, $B_3 = (0,0)$, $B_4 = (1,0)$, $B_5 = (1,1)$, $B_6 = (-1,1)$. The domain Ω_1 is divided by using some finite element partitions including uniform triangular partitions "mesh 135", uniform rectangular partitions, randomized quadrilateral partitions, hexagonal partitions and octagonal partitions. The polygonal meshes are generated by PolyMesher package [32] (see Figure 1) and refined by Lloyd iterations. The uniform triangular partitions are employed to divide the domain Ω_2.

TABLE 1. Errors and convergence rates for the linear element; exact solution $u = \cos(x+1)\sin(2y-1)$ on the uniform triangular partitions in Ω_1.

α	$1/h$	$\|\|\|e_h\|\|\|$	$\|e_0\|$	$\|e_b\|_{\mathcal{E}_h}$	$\|e_b\|_{\partial\Omega}$	$\|e_b\|_{L^1(\partial\Omega)}$	$\|e_b\|_{\infty,\partial\Omega}$
	8	3.86E-01	6.29E-02	7.67E-02	1.15E-01	1.95E-01	1.18E-01
1	16	2.95E-01	3.57E-02	4.29E-02	6.67E-02	1.12E-01	7.16E-02
	32	2.18E-01	1.94E-02	2.30E-02	3.65E-02	6.06E-02	3.98E-02
	64	1.59E-01	1.02E-02	1.19E-02	1.92E-02	3.16E-02	2.14E-02
	128	1.14E-01	5.25E-03	6.10E-03	9.89E-03	1.62E-02	1.13E-02
Rate		0.48	0.96	0.97	0.96	0.97	0.92
	8	1.67E-01	1.47E-02	1.29E-02	1.90E-02	3.14E-02	2.09E-02
2	16	8.62E-02	3.73E-03	3.26E-03	5.02E-03	8.15E-03	5.84E-03
	32	4.35E-02	9.37E-04	8.12E-04	1.28E-03	2.06E-03	1.53E-03
	64	2.18E-02	2.35E-04	2.02E-04	3.20E-04	5.16E-04	3.92E-04
	128	1.09E-02	5.87E-05	5.03E-05	8.02E-05	1.29E-04	9.92E-05
Rate		1.00	2.00	2.00	2.00	2.00	1.98
	8	8.12E-02	1.19E-02	3.46E-03	2.51E-03	4.08E-03	2.82E-03
3	16	3.57E-02	3.02E-03	8.16E-04	3.19E-04	5.15E-04	3.79E-04
	32	1.64E-02	7.59E-04	2.02E-04	4.01E-05	6.45E-05	4.88E-05
	64	7.79E-03	1.90E-04	5.05E-05	5.01E-06	8.07E-06	6.18E-06
	128	3.79E-03	4.77E-05	1.26E-05	6.27E-07	1.01E-06	7.78E-07
Rate		1.04	2.00	2.00	3.00	3.00	2.99

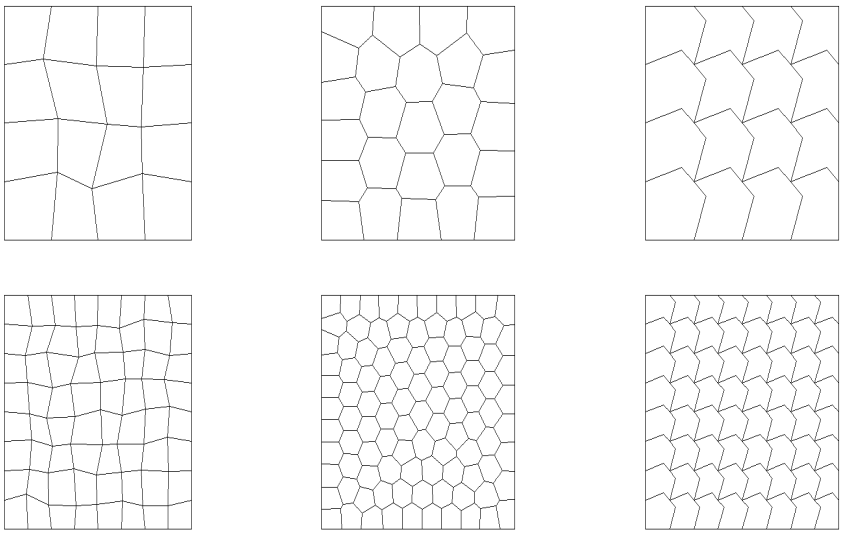

FIGURE 1. Mesh level 1 (top) and mesh level 2 (bottom) of the randomised quadrilateral partitions, the hexagonal partitions and the non-convex octagonal partitions from left to right, respectively.

TABLE 2. Errors and convergence rates for the quadratic element; exact solution $u = \cos(x+1)\sin(2y-1)$ on the uniform triangular partitions in Ω_1.

α	$1/h$	$\|\|\|e_h\|\|\|$	$\|e_0\|$	$\|e_b\|_{\mathcal{E}_h}$	$\|e_b\|_{\partial\Omega}$	$\|e_b\|_{L^1(\partial\Omega)}$	$\|e_b\|_{\infty,\partial\Omega}$
	8	6.82E-02	4.27E-03	5.42E-03	8.43E-03	2.06E-02	5.28E-03
2	16	3.45E-02	1.08E-03	1.31E-03	2.15E-03	5.23E-03	1.41E-03
	32	1.73E-02	2.71E-04	3.20E-04	5.40E-04	1.31E-03	3.63E-04
	64	8.65E-03	6.77E-05	7.91E-05	1.35E-04	3.28E-04	9.21E-05
	128	4.33E-03	1.69E-05	1.97E-05	3.38E-05	8.20E-05	2.32E-05
Rate		1.00	2.00	2.00	2.00	2.00	1.99
	8	2.45E-02	5.75E-04	7.02E-04	1.07E-03	2.61E-03	6.96E-04
3	16	8.67E-03	7.44E-05	8.65E-05	1.35E-04	3.28E-04	9.06E-05
	32	3.06E-03	9.47E-06	1.08E-05	1.69E-05	4.10E-05	1.15E-05
	64	1.08E-03	1.20E-06	1.35E-06	2.11E-06	5.12E-06	1.45E-06
	128	3.83E-04	1.50E-07	1.68E-07	2.64E-07	6.41E-07	1.82E-07
Rate		1.50	2.99	3.00	3.00	3.00	2.99
	8	8.99E-03	2.82E-04	2.76E-04	1.35E-04	3.27E-04	8.78E-05
4	16	2.26E-03	3.63E-05	3.54E-05	8.44E-06	2.05E-05	5.67E-06
	32	5.65E-04	4.59E-06	4.50E-06	5.28E-07	1.28E-06	3.60E-07
	64	1.41E-04	5.77E-07	5.66E-07	3.30E-08	8.01E-08	2.26E-08
	128	3.54E-05	7.23E-08	7.10E-08	2.06E-09	5.00E-09	1.42E-09
Rate		2.00	3.00	3.00	4.00	4.00	4.00
	8	4.00E-03	2.84E-04	2.75E-04	1.68E-05	4.09E-05	1.10E-05
5	16	8.50E-04	3.63E-05	3.55E-05	5.28E-07	1.28E-06	3.55E-07
	32	1.91E-04	4.59E-06	4.50E-06	1.65E-08	4.00E-08	1.12E-08
	64	4.47E-05	5.77E-07	5.66E-07	5.16E-010	1.25E-09	3.54E-010
	128	1.08E-05	7.23E-08	7.10E-08	1.61E-011	3.91E-011	1.11E-011
Rate		2.05	3.00	3.00	5.00	5.00	5.00

In addition to $|||e_h|||$, $\|e_0\|$ and $\|e_b\|_{\mathcal{E}_h}$, the following metrics are employed to measure e_b :

$$\|e_b\|_{\partial\Omega} = \Big(\sum_{e\in\mathcal{E}_{\partial\Omega}} \int_e |Q_b u - u_b|^2 ds \Big)^{\frac{1}{2}}, \ \|e_b\|_{L^1(\partial\Omega)} = \sum_{e\in\mathcal{E}_{\partial\Omega}} \int_e |Q_b u - u_b| ds,$$

$$\|e_b\|_{\infty,\partial\Omega} = \max_{\substack{(x,y)\in e \\ e\in\mathcal{E}_{\partial\Omega}}} |Q_b u(x,y) - u_b(x,y)|,$$

TABLE 3. Errors and convergence rates for the linear element; exact solution $u = \exp(2x)\cos(3y)$ on the polygonal partitions in Ω_1.

h	Dof	$\|\|\|e_h\|\|\|$	$\|e_0\|$	$\|e_b\|_{\mathcal{E}_h}$	$\|e_b\|_{\partial\Omega}$	$\|e_b\|_{L^1(\partial\Omega)}$	$\|e_b\|_{\infty,\partial\Omega}$
		Randomised quadrilateral partitions					
0.114	544	1.15E-00	2.35E-02	5.21E-02	6.78E-02	8.27E-02	8.91E-02
0.0594	2112	6.05E-01	6.59E-03	1.39E-02	1.87E-02	2.18E-02	2.57E-02
0.0302	8320	3.07E-01	1.70E-03	3.55E-03	4.87E-03	5.55E-03	6.82E-03
0.0152	33024	1.55E-01	4.31E-04	8.93E-04	1.23E-03	1.39E-03	1.74E-03
Rate		1.00	1.98	2.01	1.99	2.02	1.95
		Hexagonal partitions					
0.0777	1200	8.02E-01	1.35E-02	3.09E-02	4.25E-02	4.91E-02	6.13E-02
0.0388	4786	4.05E-01	3.23E-03	7.36E-03	1.09E-02	1.22E-02	1.67E-02
0.0194	19160	1.99E-01	7.69E-04	1.74E-03	2.63E-03	2.97E-03	4.04E-03
0.00946	76661	9.82E-02	1.87E-04	4.13E-04	6.50E-04	7.31E-04	1.05E-03
Rate		1.00	2.03	2.05	1.99	2.00	1.94
		Non-octagonal partitions					
0.182	288	1.65E-00	6.41E-02	9.19E-02	1.01E-01	1.30E-01	1.38E-01
0.0911	1088	9.05E-01	1.79E-02	2.77E-02	2.80E-02	3.33E-02	3.87E-02
0.0456	4224	4.70E-01	4.74E-03	7.51E-03	7.27E-03	8.37E-03	1.02E-02
0.0228	16640	2.38E-01	1.22E-03	1.94E-03	1.84E-03	2.09E-03	2.60E-03
Rate		0.93	1.91	1.86	1.93	1.99	1.91

TABLE 4. Errors and convergence rates for the quadratic element; exact solution $u = \cos(\pi x)\cos(\pi y)$ on the uniform triangular partitions in Ω_1.

α	$1/h$	$\|\|\|e_h\|\|\|$	$\|e_0\|$	$\|e_b\|_{\mathcal{E}_h}$	$\|e_b\|_{\partial\Omega}$	$\|e_b\|_{L^1(\partial\Omega)}$	$\|e_b\|_{\infty,\partial\Omega}$
	8	2.85E-02	3.30E-03	3.23E-03	1.16E-03	2.94E-03	5.88E-04
0	16	7.19E-03	4.12E-04	4.10E-04	1.59E-04	4.04E-04	7.99E-05
	32	1.80E-03	5.15E-05	5.14E-05	2.08E-05	5.29E-05	1.04E-05
	64	4.51E-04	6.44E-06	6.43E-06	2.65E-06	6.75E-06	1.33E-06
	128	1.13E-04	8.04E-07	8.04E-07	3.35E-07	8.53E-07	1.68E-07
Rate		2.00	3.00	3.00	2.98	2.98	2.99
	8	2.84E-02	3.27E-03	3.17E-03	5.71E-04	1.45E-03	2.88E-04
1	16	7.18E-03	4.10E-04	4.06E-04	7.22E-05	1.83E-04	3.62E-05
	32	1.80E-03	5.14E-05	5.11E-05	9.04E-06	2.30E-05	4.52E-06
	64	4.51E-04	6.43E-06	6.41E-06	1.13E-06	2.88E-06	5.66E-07
	128	1.13E-04	8.04E-07	8.02E-07	1.41E-07	3.60E-07	7.07E-08
Rate		2.00	3.00	3.00	3.00	3.00	3.00
	8	2.84E-02	3.26E-03	3.14E-03	1.13E-04	2.86E-04	5.71E-05
2	16	7.17E-03	4.09E-04	4.03E-04	7.42E-06	1.89E-05	3.72E-06
	32	1.80E-03	5.13E-05	5.10E-05	4.75E-07	1.21E-06	2.37E-07
	64	4.50E-04	6.42E-06	6.40E-06	3.00E-08	7.64E-08	1.50E-08
	128	1.13E-04	8.04E-07	8.02E-07	1.89E-09	4.80E-09	9.43E-010
Rate		2.00	3.00	3.00	3.99	3.99	3.99
	8	2.84E-02	3.25E-03	3.14E-03	1.53E-05	3.85E-05	7.70E-06
3	16	7.17E-03	4.09E-04	4.03E-04	4.83E-07	1.23E-06	2.42E-07
	32	1.80E-03	5.13E-05	5.10E-05	1.52E-08	3.86E-08	7.58E-09
	64	4.50E-04	6.42E-06	6.40E-06	4.74E-010	1.21E-09	2.37E-010
	128	1.13E-04	8.04E-07	8.02E-07	1.48E-011	3.77E-011	7.40E-012
Rate		2.00	3.00	3.00	5.00	5.00	5.00

for the linear finite element the maximum norm $\|e_b\|_{\infty,\partial\Omega}$ is calculated over the midpoint of each edge, and for the quadratic finite element the maximum norm $\|e_b\|_{\infty,\partial\Omega}$ is calculated over the the starting point and ending point of each edge in two dimensions.

8.1. Smooth Solutions. The first part is to numerically validate the accuracy of WG scheme (7) for the equation (1) with smooth solutions on the square domain Ω_1. The diffusion tensor $a = \{a_{ij}\}_{i,j=1}^2$ is chosen as the variable coefficient matrix in Table 1 and the identity matrix in Tables 2-5.

TABLE 5. Errors and convergence rates for the quadratic element; exact solution $u = \cos(x+1)\sin(2y-1)$ on the uniform rectangular partitions in Ω_1.

	$1/h$	$\|\|\|e_h\|\|\|$	$\|e_0\|$	$\|e_b\|_{\mathcal{E}_h}$	$\|e_b\|_{\partial\Omega}$	$\|e_b\|_{L^1(\partial\Omega)}$	$\|e_b\|_{\infty,\partial\Omega}$
	8	8.72E-03	9.90E-05	1.51E-04	1.35E-04	3.28E-04	8.78E-05
Type 1	16	2.19E-03	9.69E-06	2.04E-05	8.44E-06	2.05E-05	5.67E-06
	32	5.49E-04	1.09E-06	2.68E-06	5.28E-07	1.28E-06	3.60E-07
	64	1.37E-04	1.31E-07	3.44E-07	3.30E-08	8.01E-08	2.26E-08
	128	3.43E-05	1.60E-08	4.36E-08	2.06E-09	5.00E-09	1.42E-09
Rate		1.99	3.02	2.98	3.99	3.99	3.99
	8	8.91E-03	1.01E-04	1.53E-04	1.48E-04	3.41E-04	1.24E-04
Type 2	16	2.23E-03	9.75E-06	2.04E-05	9.21E-06	2.13E-05	7.84E-06
	32	5.59E-04	1.09E-06	2.68E-06	5.75E-07	1.33E-06	4.93E-07
	64	1.40E-04	1.31E-07	3.44E-07	3.59E-08	8.33E-08	3.09E-08
	128	3.50E-05	1.60E-08	4.36E-08	2.25E-09	5.21E-09	1.94E-09
Rate		1.99	3.02	2.98	4.00	4.00	3.99
	8	8.75E-03	9.96E-05	1.51E-04	1.37E-04	3.28E-04	9.34E-05
Type 3	16	2.19E-03	9.70E-06	2.04E-05	8.47E-06	2.05E-05	5.84E-06
	32	5.49E-04	1.09E-06	2.68E-06	5.29E-07	1.28E-06	3.65E-07
	64	1.37E-04	1.31E-07	3.44E-07	3.30E-08	8.01E-08	2.28E-08
	128	3.43E-05	1.60E-08	4.36E-08	2.06E-09	5.00E-09	1.43E-09
Rate		1.99	3.02	2.98	4.00	4.00	4.00

Table 1 demonstrates the numerical performance of the linear WG element for the equation (1) in Ω_1 with different values of α on the uniform triangular partitions. The variable diffusion tensor a is given by $a_{11} = 1 + x^2$, $a_{12} = a_{21} = xy/4$ and $a_{22} = 1 + y^2$. The exact solution is $u = \cos(x + 1)\sin(2y - 1)$. These numerical results are in perfect consistency with the theoretical results. Moreover, for the case of $\alpha = 3$, the rates of convergence for $|||e_h|||$, $\|e_0\|$ and $\|e_b\|_{\mathcal{E}_h}$ remain to be of orders $\mathcal{O}(h)$, $\mathcal{O}(h)$ and $\mathcal{O}(h^2)$, respectively. Therefore, we recommend the value of $\alpha = 2$ in practice. In addition, the numerical performance of the errors $\|e_b\|_{\partial\Omega}$, $\|e_b\|_{L^1(\partial\Omega)}$ and $\|e_b\|_{\infty,\partial\Omega}$ supports strongly our expectations.

Table 2 lists some numerical results for the quadratic WG element with different values of α. The exact solution is $u = \cos(x + 1)\sin(2y - 1)$. We observe that the convergence rate for $|||e_h|||$ is in perfect consistent with theoretical predictions. For the numerical errors $\|e_0\|$ and $\|e_b\|_{\mathcal{E}_h}$, the numerical results are consistent with the theory for $\alpha = 2, 4, 5$, but greatly outperform the theory for the value of $\alpha = 3$. In addition, the same rates of convergence are observed of $|||e_h|||$, $\|e_0\|$ and $\|e_b\|_{\mathcal{E}_h}$ although the parameter $\alpha = 5$ exceeds the theoretical optimal exponent $\alpha = 4$. Thus, $\alpha = 4$ is recommended in practical computing. Once again, the numerical errors $\|e_b\|_{\partial\Omega}$, $\|e_b\|_{L^1(\partial\Omega)}$ and $\|e_b\|_{\infty,\partial\Omega}$ confirm greatly our prediction of $\mathcal{O}(h^\alpha)$.

Table 3 presents some numerical results for the linear WG element on different types of polygonal meshes shown in Figure 1. The parameter is set as the optimal parameter $\alpha = 2$. It is clearly seen that these numerical results achieve the optimal orders of convergence for numerical errors $|||e_h|||$, $\|e_0\|$ and $\|e_b\|_{\mathcal{E}_h}$. It should be pointed out that the convergence rates are computed by the least-square approach.

Table 4 illustrates the numerical performance of the quadratic WG element with different values of α. The exact solution is given by $u = \cos(\pi x)\cos(\pi y)$, which satisfies $a\nabla u \cdot \mathbf{n} = 0$ on $\partial\Omega$. From the comparison, these numerical results typically outperform the theoretical prediction especially for the values of $\alpha = 0$ and $\alpha = 1$. Moreover, the errors $\|e_b\|_{\partial\Omega}$, $\|e_b\|_{L^1(\partial\Omega)}$ and $\|e_b\|_{\infty,\partial\Omega}$ seem to exceed our expectation.

Table 5 reports some numerical results for the quadratic WG element with three types of the uniform rectangular mesh. The optimal exponent $\alpha = 4$ is employed.

TABLE 6. Errors and convergence rates for the linear element and quadratic element; exact solution $u = (x^2+y^2)^{\frac{1}{4}}\sin(2\arctan(\frac{y}{x}))$ on the uniform triangular partitions in Ω_2.

	$k=1,\alpha=2$					
$1/h$	$\|\|\|e_h\|\|\|$	Rate	$\|e_0\|$	Rate	$\|e_b\|_{\mathcal{E}_h}$	Rate
16	7.03E-01	0.74	4.12E-02	1.59	5.22E-02	1.60
32	4.35E-01	0.69	1.41E-02	1.55	1.81E-02	1.53
64	2.80E-01	0.63	4.97E-03	1.50	6.62E-03	1.45
128	1.87E-01	0.59	1.82E-03	1.45	2.56E-03	1.37
$1/h$	$\|e_b\|_{\partial\Omega}$	Rate	$\|e_b\|_{L^1(\partial\Omega)}$	Rate	$\|e_b\|_{\infty,\partial\Omega}$	Rate
16	3.15E-02	1.89	3.56E-02	2.00	7.34E-02	1.44
32	8.31E-03	1.92	8.85E-03	2.01	2.65E-02	1.47
64	2.17E-03	1.94	2.20E-03	2.01	9.45E-03	1.49
128	5.62E-04	1.95	5.47E-04	2.01	3.36E-03	1.49
	$k=1,\alpha=3$					
$1/h$	$\|\|\|e_h\|\|\|$	Rate	$\|e_0\|$	Rate	$\|e_b\|_{\mathcal{E}_h}$	Rate
16	5.00E-01	0.61	3.19E-02	1.50	2.69E-02	1.36
32	3.47E-01	0.53	1.16E-02	1.46	1.11E-02	1.27
64	2.44E-01	0.51	4.31E-03	1.43	4.75E-03	1.23
128	1.72E-01	0.50	1.64E-03	1.40	2.06E-03	1.20
$1/h$	$\|e_b\|_{\partial\Omega}$	Rate	$\|e_b\|_{L^1(\partial\Omega)}$	Rate	$\|e_b\|_{\infty,\partial\Omega}$	Rate
16	2.01E-03	2.93	2.24E-03	3.02	4.76E-03	2.49
32	2.62E-04	2.94	2.77E-04	3.01	8.43E-04	2.50
64	3.40E-05	2.95	3.44E-05	3.01	1.49E-04	2.50
128	4.40E-06	2.95	4.27E-06	3.01	2.64E-05	2.50
	$k=2,\alpha=3$					
$1/h$	$\|\|\|e_h\|\|\|$	Rate	$\|e_0\|$	Rate	$\|e_b\|_{\mathcal{E}_h}$	Rate
16	2.43E-01	0.73	6.63E-02	1.50	1.92E-02	1.44
32	1.63E-01	0.58	2.36E-02	1.49	7.81E-03	1.30
64	1.13E-01	0.52	8.51E-03	1.47	3.32E-03	1.23
128	7.99E-02	0.51	3.09E-03	1.46	1.44E-03	1.20
$1/h$	$\|e_b\|_{\partial\Omega}$	Rate	$\|e_b\|_{L^1(\partial\Omega)}$	Rate	$\|e_b\|_{\infty,\partial\Omega}$	Rate
16	1.43E-03	2.93	2.24E-03	3.02	2.96E-03	2.49
32	1.86E-04	2.94	2.77E-04	3.01	5.25E-04	2.50
64	2.41E-05	2.95	3.44E-05	3.01	9.28E-05	2.50
128	3.12E-06	2.95	4.28E-06	3.01	1.64E-05	2.50
	$k=2,\alpha=4$					
$1/h$	$\|\|\|e_h\|\|\|$	Rate	$\|e_0\|$	Rate	$\|e_b\|_{\mathcal{E}_h}$	Rate
16	2.27E-01	0.54	6.60E-02	1.49	1.81E-02	1.29
32	1.60E-01	0.51	2.36E-02	1.48	7.65E-03	1.24
64	1.13E-01	0.50	8.50E-03	1.47	3.30E-03	1.21
128	7.98E-02	0.50	3.09E-03	1.46	1.44E-03	1.20
$1/h$	$\|e_b\|_{\partial\Omega}$	Rate	$\|e_b\|_{L^1(\partial\Omega)}$	Rate	$\|e_b\|_{\infty,\partial\Omega}$	Rate
16	8.94E-05	3.94	1.40E-04	4.02	1.86E-04	3.50
32	5.81E-06	3.94	8.66E-06	4.01	1.64E-05	3.50
64	3.77E-07	3.95	5.37E-07	4.01	1.45E-06	3.50
128	2.43E-08	3.95	3.34E-08	4.01	1.28E-07	3.50

We denote by arbitrary edge e_{ij} on $\partial\Omega$ forming by the starting point $A_i = (x_i, y_i)$ and ending point $A_j = (x_j, y_j)$. Here three types of discrete points are given by $\{A_i, A_j\}$, $\{\frac{1}{8}(A_i + A_j), \frac{3}{4}(A_i + A_j)\}$ and the two Gaussian quadrature points, respectively. These numerical results suggest that the optimal orders of convergence for the numerical errors $|\!|\!|e_h|\!|\!|$, $\|e_0\|$ and $\|e_b\|_{\mathcal{E}_h}$ are perfectly confirmed. Once again, the convergence rates for the numerical errors $\|e_b\|_{\partial\Omega}$, $\|e_b\|_{L^1(\partial\Omega)}$ and $\|e_b\|_{\infty,\partial\Omega}$ reach our expectation.

8.2. Low Regularity Solutions. To numerically explore the performance of the WG scheme (7) for the equation (1) with low regularity solutions, some numerical results are presented on the general polygonal partitions. The diffusion tensor a is identity matrix.

Table 6 presents some numerical results for the linear and quadratic WG elements with different values of α on the uniform triangular partitions. The exact solution

TABLE 7. Errors and convergence rates for the linear element; exact solution $u = -x(1-x)y(1-y)(x^2+y^2)^{\frac{2/5-2}{2}}$ on the polygonal partitions in Ω_1.

h	Dof	$\|\|\|e_h\|\|\|$	$\|e_0\|$	$\|e_b\|_{\mathcal{E}_h}$	$\|e_b\|_{\partial\Omega}$	$\|e_b\|_{L^1(\partial\Omega)}$	$\|e_b\|_{\infty,\partial\Omega}$
		Uniform triangular partitions					
1/32	3136	1.54E-01	3.87E-02	3.29E-03	1.74E-04	1.15E-04	6.39E-04
1/64	12416	1.14E-01	1.47E-02	1.25E-03	2.39E-05	1.45E-05	1.22E-04
1/128	49408	8.63E-02	5.56E-03	4.73E-04	3.28E-06	1.81E-06	2.31E-05
1/256	197120	6.53E-02	2.11E-03	1.79E-04	4.48E-07	2.27E-07	4.39E-06
Rate		0.41	1.40	1.40	2.87	2.99	2.40
		Uniform rectangular partitions					
1/32	3152	1.10E-01	5.08E-03	1.98E-03	1.45E-04	9.48E-05	5.79E-04
1/64	12448	8.22E-02	1.93E-03	7.62E-04	2.00E-05	1.19E-05	1.10E-04
1/128	49472	6.21E-02	7.31E-04	2.90E-04	2.74E-06	1.50E-06	2.09E-05
1/256	197248	4.71E-02	2.77E-04	1.10E-04	3.75E-07	1.77E-07	3.96E-06
Rate		0.41	1.40	1.39	2.87	3.02	2.40
		Randomised quadrilateral partitions					
0.114	544	1.55E-01	1.55E-02	4.17E-03	3.48E-03	2.83E-03	8.95E-03
0.0594	2112	8.95E-02	5.84E-03	1.63E-03	5.28E-04	3.91E-04	1.86E-03
0.0302	8320	6.01E-02	2.25E-03	6.18E-04	7.57E-05	5.17E-05	3.62E-04
0.0152	33024	4.60E-02	7.88E-04	2.46E-04	1.06E-05	6.62E-06	7.07E-05
Rate		0.60	1.47	1.40	2.87	3.00	2.40
		Hexagonal partitions					
0.0777	1200	1.50E-01	1.89E-02	5.67E-03	1.42E-03	1.17E-03	3.75E-03
0.0388	4786	1.01E-01	7.26E-03	2.07E-03	2.00E-04	1.49E-04	7.26E-04
0.0194	19160	5.50E-02	2.61E-03	5.19E-04	2.59E-05	1.78E-05	1.33E-04
0.0095	76661	4.66E-02	1.01E-03	2.28E-04	3.50E-06	2.14E-06	2.48E-05
Rate		0.59	1.40	1.57	2.86	3.00	2.39
		Non-octagonal partitions					
0.182	288	2.10E-01	4.13E-02	8.68E-03	7.73E-03	6.95E-03	1.56E-02
0.0911	1088	1.30E-01	1.55E-02	3.62E-03	1.11E-03	9.01E-04	3.01E-03
0.0456	4224	9.61E-02	5.89E-03	1.47E-03	1.56E-04	1.16E-04	5.75E-04
0.0228	16640	7.47E-02	2.25E-03	5.77E-04	2.17E-05	1.47E-05	1.09E-04
Rate		0.49	1.40	1.30	2.83	2.96	2.39

is $u = (x^2+y^2)^{\frac{1}{4}}\sin(2\arctan(\frac{y}{x}))$ on the L-shaped domain Ω_2. It is easy to check $u \in H^{1.5-\varepsilon}$ for arbitrary small $\varepsilon > 0$. For $|\!|\!|e_h|\!|\!|$, $\|e_0\|$ and $\|e_b\|_{\mathcal{E}_h}$, the numerical results for the linear element with $\alpha = 3$ is more stable than that for linear element with $\alpha = 2$. For the quadratic WG element with $\alpha = 2$ or $\alpha = 3$, the rates of convergence for $|\!|\!|e_h|\!|\!|$, $\|e_0\|$ and $\|e_b\|_{\mathcal{E}_h}$ seem to be around $\mathcal{O}(h^{0.5})$, $\mathcal{O}(h^{1.5})$ and $\mathcal{O}(h^{1.2})$, respectively. Moreover, $\|e_b\|_{\partial\Omega}$, $\|e_b\|_{L^1(\partial\Omega)}$ and $\|e_b\|_{\infty,\partial\Omega}$ converge to zero at the rates of $\mathcal{O}(h^{\alpha})$, $\mathcal{O}(h^{\alpha})$ and $\mathcal{O}(h^{\alpha-0.5})$, respectively.

Tables 7-8 illustrate the numerical performance of the linear WG element with $\alpha = 3$ on different types of polygonal partitions shown in Figure 1. The right-hand side function f is chosen for exact solution $u = -x(1-x)y(1-y)(x^2+y^2)^{\frac{2/5-2}{2}}$. It is obvious that $f \leq 0$ in Ω_1 and the exact solution u has the regularity of $u \in H^{1+\frac{2}{5}-\varepsilon}(\Omega)$ for arbitrary small $\varepsilon > 0$. We observe from Table 7 that on the uniform triangular partitions and uniform rectangular partitions, the rates of convergence for $|\!|\!|e_h|\!|\!|$, $\|e_0\|$, $\|e_b\|_{\mathcal{E}_h}$, $\|e_b\|_{\partial\Omega}$, $\|e_b\|_{L^1(\partial\Omega)}$ and $\|e_b\|_{\infty,\partial\Omega}$ are of orders $\mathcal{O}(h^{0.4})$, $\mathcal{O}(h^{1.4})$, $\mathcal{O}(h^{1.4})$, $\mathcal{O}(h^{2.87})$, $\mathcal{O}(h^{3})$, $\mathcal{O}(h^{2.4})$, respectively. Moreover, the performance of numerical approximation on the polygonal partitions is presented in Table 7. Table 8 reports the maximum values of the numerical approximation u_b on different polygonal partitions. We observe that $\max_{x\in\Omega\setminus\partial\Omega} u_b(x,y) < \max_{x\in\partial\Omega} u_b(x,y)$. This indicates the maximum principle holds true for the numerical solution u_b on the polygonal partitions, for which the mathematical theory has not been developed yet.

TABLE 8. The discrete maximum values of the WG solution u_b; exact solution $u = -x(1-x)y(1-y)(x^2+y^2)^{\frac{2/5-2}{2}}$ on the polygonal partitions in Ω_1.

h	Uniform triangular partitions		
	1/64	1/128	1/256
$\max_{\Omega\setminus\partial\Omega} u_b(x,y)$	-3.499E-05	-8.755E-06	-2.19E-06
$\max_{\partial\Omega} u_b(x,y)$	-1.709E-08	-1.069E-09	-6.68E-011
h	Uniform rectangular partitions		
	1/64	1/128	1/256
$\max_{\Omega\setminus\partial\Omega} u_b(x,y)$	-4.665E-05	-1.168E-05	-2.920E-06
$\max_{\partial\Omega} u_b(x,y)$	-7.620E-09	-4.760E-010	-2.973E-011
h	Randomised quadrilateral partitions		
	0.0594	0.0302	0.0152
$\max_{\Omega\setminus\partial\Omega} u_b(x,y)$	-2.679E-04	-6.261E-05	-1.523E-05
$\max_{\partial\Omega} u_b(x,y)$	-1.052E-06	-6.211E-08	-3.977E-09
h	Hexagonal partitions		
	0.0388	0.0194	0.00946
$\max_{\Omega\setminus\partial\Omega} u_b(x,y)$	-1.072E-04	-3.410E-05	-9.240E-06
$\max_{\partial\Omega} u_b(x,y)$	-1.487E-07	-1.422E-08	-7.615E-010
h	Non-octagonal partitions		
	0.0911	0.0456	0.0228
$\max_{\Omega\setminus\partial\Omega} u_b(x,y)$	-4.335E-05	-8.250E-06	-2.072E-06
$\max_{\partial\Omega} u_b(x,y)$	-3.165E-06	-1.982E-07	-1.239E-08

9. Conclusions

In this paper, we have developed a new WG method with weakly enforced Dirichlet boundary condition for the second order elliptic equation. Two additional bilinear forms are incorporated into the weak Galerkin framework to weakly enforce the Dirichlet boundary condition. Optimal order error estimates for the numerical approximation are rigorously established. Some numerical experiments are reported to validate the developed theory. The last numerical experiment also reveals that the maximum principle holds true for the WG scheme (7) on general polytopal meshes. To examine the numerical method proposed in this paper, more realistic problems like the wall-bounded turbulent flows will be numerical solved and analyzed theoretically in the future work.

Acknowledgments

The authors appreciate the financial supports provided by National Key R&D Program of China (No. 2020YFA0713603) and Key R&D Program of Shandong Province of China(No. 2020CXGC010101).

References

[1] L. B. D. Veiga, F. Brezzi, L. D. Marini and A. Russo, Virtual element method for general second-order elliptic problems on polygonal meshes, Math. Models Methods Appl. Sci., vol. 26(4), pp. 729-750, 2016.

[2] L. B. D. Veiga, F. Brezzi, A. Cangiani, L. D. Marini and A. Russo, Basic principles of virtual element methods, Math. Models Methods Appl. Sci., vol. 23(1), pp. 199-214, 2013.

[3] S. C. Brenner and L. R. Scott, The mathematical theory of finite element methods, 3rd ed., Texts Appl. Math. 15, Springer, New York, 2008.

[4] S. Bertoluzza, M. Pennacchio and D. Prada, Weakly imposed Dirichlet boundary conditions for 2D and 3D virtual elements, Comput. Methods Appl. Mech. Engrg., vol. 400, pp. 115454, 2022.
[5] I. Babuška, The finite element method with penalty, Math. Comp., vol. 27(122), pp. 221-228, 1973.
[6] I. Babuška, The finite element method with Lagrangian multipliers, Numer. Math., vol. 20, pp. 179-192, 1973.
[7] Y. Bazilevs, C. Michler, V. M. Calo and T. J. R. Hughes, Isogeometric variational multiscale modeling of wall-bounded turbulent flows with weakly enforced boundary conditions on unstretched meshes, Comput. Methods Appl. Mech. Engrg., vol. 199, pp. 780-790, 2010.
[8] Y. Bazilevs, C. Michler, V. M. Calo and T. J. R. Hughes, Weak Dirichlet boundary conditions for wall-bounded turbulent flows, Comput. Methods Appl. Mech. Engrg., vol. 196, pp. 4853-4862, 2007.
[9] B. Cockburn, J. Gopalakrishnan and R. Lazarov, Unified hybridization of discontinuous Galerkin, mixed, and continuous Galerkin methods for second order elliptic problems, SIAM J. Numer. Anal., vol. 47(2), pp. 1319-1365, 2009.
[10] S. Cao, C. Wang and J. Wang, A new numerical method for div-curl systems with low regularity assumptions, Comput. Math. Appl., vol. 114, pp. 47-59, 2022.
[11] W. Cao, C. Wang and J. Wang, An L^p-weak Galerkin method for second order elliptic equations in non-divergence, https://arxiv.org/pdf/2106.03191v1.pdf.
[12] K. L. Cascavita, F. Chouly and A. Ern, Hybrid high-order discretizations combined with Nitsche's method for Dirichlet and Signorini boundary conditions, IMA. J. Numer. Anal., vol. 40, pp. 2189-2226, 2020.
[13] V. Ginting, G. Lin and J. Liu, On application of the weak Galerkin finite element method to a two-phase model for subsurface flow, J. Sci. Comput., vol. 66, pp. 225-239, 2016.
[14] F. Gao, S. Zhang and P. Zhu, Modified weak Galerkin method with weakly imposed boundary condition for convection-dominated diffusion equations, Appl. Numer. Math., vol. 157, pp. 490-504, 2020.
[15] Y. Huang, J. Li and D. Li, Developing weak Galerkin finite element methods for the wave equation, Numer. Methods Partial Differ. Equ., vol. 33(3), pp. 868-884, 2017.
[16] X. Hu, L. Mu and X. Ye, A weak Galerkin finite element method for the Navier-Stokes equations, J. Comput. Appl. Math., vol. 362, pp. 614-625, 2019.
[17] M. C. Hsu, I. Akkerman and Y. Bazilevs, Wind turbine aerodynamics using ALECVMS: validation and the role of weakly enforced boundary conditions, Comput. Mech., vol. 50, pp. 499-511, 2012.
[18] R. Lin, X. Ye, S. Zhang and P. Zhu, A weak Galerkin finite element method for singular perturbed convection-diffusion reaction problems, SIAM J. Numer. Anal., vol. 56(3), pp. 1482-1497, 2018.
[19] Y. Liu and J. Wang, A primal-dual weak Galerkin method for div-curl systems with low-regularity solutions, https://arxiv.org/pdf/2003.11795v2.pdf.
[20] Y. Liu and J. Wang, A locking-free P_0 finite element method for linear elasticity equations on polytopal partitions, IMA. J. Numer. Anal., vol. 0, pp. 1-35, 2021.
[21] A. J. Lew and G. C. Buscaglia, A discontinuous-Galerkin-based immersed boundary method, Int. J. Numer. Methods Engrg., vol. 76(4), pp. 427-454, 2008.
[22] L. Mu, J. Wang and X. Ye, A weak Galerkin finite element method with polynomial reduction, J. Comput. Appl. Math., vol. 285, pp. 45-58, 2015.
[23] L. Mu, J. Wang, Y. Wang and X. Ye, A stable numerical algorithm for the Brinkman equations by weak Galerkin finite element methods, J. Comput. Phys., vol. 273, pp. 327-342, 2014.
[24] L. Mu, J. Wang, X. Ye and S. Zhao, A new weak Galerkin finite element method for elliptic interface problems, J. Comput. Phys., vol. 325, pp. 157-173, 2016.
[25] L. Mu, J. Wang, X. Ye and S. Zhang, A weak Galerkin finite element mthod for the Maxwell equations, J. Sci. Comput., vol. 65, pp. 363-386, 2015.
[26] L. Mu, X. Ye and S. Zhang, A stabilizer-free, pressure-robust, and superconvergence weak Galerkin finite element method for the Stokes equations on polytopal mesh, SIAM J. Sci. Comput., vol. 43(4), pp. A2614-A2637, 2021.
[27] N. Moës, E. Béchet and M. Tourbier, Imposing Dirichlet boundary conditions in the extended finite element method, Int. J. Numer. Meth. Engng., vol. 67, pp. 1641-1669, 2006.

[28] J. Nitsche, Über ein variationsprinzip zur Lösung von Dirichlet-problemen bei Verwendung von Teilraumen, die keinen Randbe-dingungen unterworfen sind, Abh. Math. Univ. Hamburg., vol. 36, pp. 9-15, 1971.
[29] D. A. D. Pietro and J. Droniou, The hybrid high-order method for polytopal meshes, design, analysis, and applications, Model. Simu. Appl., vol. 19, 2019.
[30] M. Ruess, D. Schillinger, Y. Bazilevs, V. Varduhn and E. Rank, *Weakly enforced essential boundary conditions for NURBS-embedded and trimmed NURBS geometries on the basis of the finite cell method*, Int. J. Numer. Meth. Engng., vol. 95, pp. 811-846, 2013.
[31] S. Shields, J. Li and E. A. Machorro, Weak Galerkin methods for time-dependent Maxwell's equations, Comput. Math. Appl., vol. 74, pp. 2106-2124, 2017.
[32] C. TAlischi, G. H. Paulino, A. Pereira and I. F. M. Menezes, PolyMesher: a general-purpose mesh generator for polygonal elements written in Matlab, Struct. Multidisc. Optim., vol. 45, pp. 309-328, 2012.
[33] A. A. Taweel, X. Wang, X. Ye and S. Zhang, A stabilizer free weak Galerkin finite element method with supercloseness of order two, Numer. Methods Partial Differ. Equ., vol. 37(2), pp. 1012-1029, 2021.
[34] J. Wang and X. Ye, A weak Galerkin finite element method for second-order elliptic problems, J. Comput. Appl. Math., vol. 241, pp. 103-115, 2013.
[35] J. Wang and R. Zhang, Maximum principles for P_1-conforming finite element approximations of quasi-linear second order elliptic equations, SIAM J. Numer. Anal., vol. 50(2), pp. 626-642, 2012.
[36] J. Wang, X. Ye and S. Zhang, Numerical investigation on weak Galerkin finite elements, Int. J. Numer. Anal. Model., vol. 17(4), pp. 517-531, 2020.
[37] J. Wang and X. Ye, A weak Galerkin mixed finite element method for second-order elliptic problems, Math. Comp., vol. 83(289), pp. 2101-2126, 2014.
[38] C. Wang and J. Wang, An efficient numerical scheme for the biharmonic equation by weak Galerkin finite element methods on polygonal or polyhedral meshes, Comput. Math. Appl., vol. 68, pp. 2314-2330, 2014.
[39] J. Wang and X. Ye, A weak Galerkin finite element method for the Stokes equations, Adv. Comput. Math., vol. 42, pp. 155-174, 2016.
[40] J. Wang, Q. Zhai, X. Ye and S. Zhang, A weak Galerkin finite element scheme for the Cahn-Hilliard equation, Math. Comp., vol. 88(315), pp. 211-235, 2019.
[41] C. Wang and J. Wang, Primal-dual weak Galerkin finite element methods for elliptic Cauchy problems, Comput. Math. Appl., vol. 79, pp. 746-763, 2020.
[42] C. Wang and J. Wang, A primal-dual weak Galerkin finite element method for second order elliptic equations in non-divergence form, Math. Comp., vol. 87, pp. 515-545, 2018.
[43] C. Wang and J. Wang, A hybridized weak Galerkin finite element method for the biharmonic equation, Int. J. Numer. Anal. Model., vol. 12(2), pp. 302-317, 2015.
[44] C. Wang and J. Wang, A primal-dual weak Galerkin finite element method for Fokker-Planck type equations, SIAM J. Numer. Anal., vol. 58(5), pp. 2632-2661, 2020.
[45] N. Wang and J. Chen, Convergence analysis on Nitsche extended finite element methods for H(curl)-elliptic interface problem, Int. J. Numer. Anal. Model., vol. 19(4), pp. 487-510, 2022.
[46] C. Wang and J. Wang, A primal-dual finite element method for first-order transport problems, J. Comput. Phys., vol. 417, pp. 109571, 2020.
[47] C. Wang, Low regularity primal-dual weak Galerkin finite element methods for ill-posed elliptic Cauchy problems, Int. J. Numer. Anal. Model., vol. 19(1), pp. 33-51, 2022.
[48] C. Wang, A modified primal-dual weak Galerkin finite element method for second order elliptic equations in non-divergence form, Int. J. Numer. Anal. Model., vol. 18(4), pp. 500-523, 2021.
[49] X. Ye and S. Zhang, A stabilizer free weak Galerkin finite element method on polytopal mesh: Part II, J. Comput. Appl. Math., vol. 394, pp. 113525, 2021.
[50] X. Ye and S. Zhang, A stabilizer free weak Galerkin finite element method on polytopal mesh: Part III, J. Comput. Appl. Math., vol. 394, pp. 113538, 2021.
[51] X. Ye and S. Zhang, A stabilizer free weak Galerkin method for the biharmonic equation on polytopal meshes, SIAM J. Numer. Anal., vol. 58(5), pp. 2572-2588, 2020.
[52] X. Ye, S. Zhang and P. Zhu, Stabilizer-free weak Galerkin methods for monotone quasilinear elliptic PDEs, Results Appl. Math., vol. 8, pp. 100097, 2020.

Research Center for Computational Science, Northwestern Polytechnical University, Xi'an, Shannxi 710129, China

E-mail: danlimath@163.com and liyiqiang@nwpu.edu.cn and yzzzb@nwpu.edu.cn